Inorganic Chemistry

ARTICLE

pubs.acs.org/IC

Multiparametric Dissolution of Thorium−Cerium Dioxide Solid Solutions

Laurent Claparede,[†,‡] Nicolas Clavier,[†] Nicolas Dacheux,[*,†] Adel Mesbah,[†] Julien Martinez,[†] Stéphanie Szenknect,[†] and Philippe Moisy[‡]

[†]ICSM, UMR 5257 CNRS/CEA/UM2/ENSCM, Site de Marcoule, Bât. 426, BP 17171, 30207 Bagnols/Cèze, France

[‡]CEA, Nuclear Energy Division, RadioChemistry & Processes Department, BP 17171, 30207 Bagnols/Cèze, France

Supporting Information

ABSTRACT: The dissolution of $Th_{1-x}Ce_xO_2$ solid solutions samples prepared by thermal conversion of oxalate precursors was studied by varying independently several parameters (such as chemical composition, leachate acidity, leaching temperature, firing temperature, and crystallization state). The relative effects of these parameters on the normalized dissolution rate were examined. Either the obtained partial order related to the proton activity ($n = 0.50 \pm 0.01$) or the activation energy ($E_A = 57 \pm 6$ kJ.mol^{-1}) suggested that the dissolution was mainly driven by surface reactions occurring at the solid/liquid interface. Conversely to that observed for $Th_{1-x}U_xO_2$ and $Ce_{1-x}Nd_xO_{2-x/2}$ solid solutions, the chemical composition did not induce strong modifications of the chemical durability of the leached samples. While the initial normalized dissolution rate slightly depended on the elimination of crystal defects for firing temperatures below 800 °C, it was mainly independent of the crystallite size ($T \geq 900$ °C). The role of crystal defects (then that of preparation conditions) appeared thus important to consider since they contributed to modifications of the normalized dissolution rates of the same order of magnitude than that of the leachate acidity.

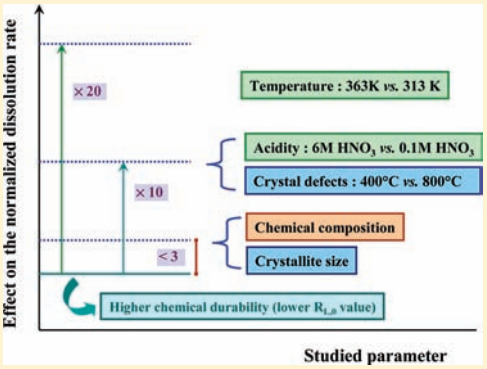

1. INTRODUCTION

Mixed actinide dioxides are currently used as fuel in pressurized water reactors (PWR) (including Gen III, EPR) and also stand as potential candidates for several Gen IV concepts including sodium-cooled fast reactor (SFR) or gas-cooled fast reactor (GFR).[1,2] Recycling of minor actinides coming from nuclear spent fuel into mixed-oxide fuels or in UO_2-based blankets surrounding the core is often considered.[3] Moreover, among several thoria applications, the most important is its potential use in nuclear energy applications. With the renewal of nuclear power, the thorium nuclear fuel cycle also received an increased interest because of several physicochemical properties (high fusion temperature, good sintering capability and resistance to radiation damages, ...) and particularly the greater thorium abundance.[4] Thoria-based fuels also provide an attractive option for the transmutation of minor actinides.[5]

In this field, the preparation of ThO_2 bearing plutonium and uranium samples was already described in literature as advanced fuel materials.[6,7] Such mixed actinide dioxides were usually prepared through dry chemistry routes based on powder mixtures which could result in some heterogeneity in the cationic distribution within the material.[8] However, wet chemistry methods were also recently proposed. They were mainly based on the precipitation of crystallized precursors[9] such as carbonates, nitrates, hydroxides, or oxalates[10−14] from aqueous solution. These latter remained probably the most frequently cited due to their quantitative precipitation and to the improvement of several properties of interest they could confer to the final ceramics (i.e., sintering capability, cationic distribution within the structure or chemical durability).[15,16]

Thorium-based dioxides are expected to have good performances in long-term storage because of very low normalized dissolution rates and low solubility.[13,17] Whereas dissolution of $Th_{1-x}U_xO_2$ was already studied by varying conventional parameters such as temperature, chemical composition or leachate acidity,[15,18−20] that of $Th_{1-x}Pu_xO_2$ and $Th_{1-x}Ce_xO_2$ (as surrogates) remains poorly known.[20]

Moreover, the consequences of the physicochemical modifications (including morphological modifications) induced by the chemical way of synthesis considered have only been recently evocated[11,13,15,21] while they would appear as key parameters either for the understanding of the reprocessing operations or for the long-term storage of spent nuclear fuel. In this field, some recent studies confirmed the significant role of several parameters such as density, porosity, grain size, or occurrence of grain boundaries on the normalized dissolution rates of $Th_{1-x}U_xO_2$ sintered samples.[15,16,22]

The aim of this paper is thus to study the dissolution of $Th_{1-x}Ce_xO_2$ solid solutions, as the first step before $Th_{1-x}Pu_xO_2$ solid solutions, through the establishment of the multiparametric

Received: August 4, 2011
Published: October 25, 2011

expression of the normalized dissolution rate then to highlight the links between the structure and the microstructure of such strongly refractory materials to dissolution and leaching. After performing the preparation of powdered $Th_{1-x}Ce_xO_2$ samples from the initial precipitation of cerium and thorium oxalates, this work was mainly focused on the study of the effects on the normalized dissolution rates of various physicochemical parameters (T, acidity) including microstructural parameters (crystallization state, crystallite size, ...).

2. DISSOLUTION OF MIXED DIOXIDES

2.1. State of Art. Some studies were already dedicated to the optimization of the operating conditions for the dissolution of PuO_2.[21,23−25] Even if the conclusions on the mechanisms involved were far less numerous, they all demonstrated the strong refractory nature of PuO_2 in both oxidative and reducing conditions.[26,27] Such property was also underlined for CeO_2, which was generally reported to be strongly resistant to corrosion in nitric acid media even if nitrate complexes played a significant role as promoting reagent for ceria dissolution.[28,29]

Rare and recent publications were focused on the discrepancies observed in the ThO_2 solubility.[17] They mainly underlined a lack of thorough solid-state analysis and pointed out the role of specific site exchange mechanisms at the solid/solution interface through experiments based on isotopic exchanges. However, the studies devoted to the links observed between physicochemical properties of the samples and their behavior during leaching tests were rarely considered while they probably exhibited an important contribution on the normalized dissolution rates.

The effect of composition was already examined for several kinds of fluorite-type systems, especially $Th_{1-x}U_xO_2$ and $Ce_{1-x}Nd_xO_{2-x/2}$. Conversely, it was not examined for $Th_{1-x}Ce_xO_2$ solid solutions to our knowledge. For both $Th_{1-x}U_xO_2$ and $Ce_{1-x}Nd_xO_{2-x/2}$ systems, the chemical composition strongly affected the chemical durability of the leached samples.[18,19,30] As instance, when dissolving $Th_{1-x}U_xO_2$ solid solutions in acid media, the direct comparison of ThO_2 and UO_2 revealed a difference of 6 orders of magnitude between the highly durable ThO_2 and the more soluble UO_2. The chemical durability of $Th_{1-x}U_xO_2$ solid-solutions was thus significantly affected by the uranium mole loading in the samples due to oxidation of tetravalent uranium into uranyl during the dissolution process. Indeed, while kinetic parameters remained almost similar to that of pure ThO_2 for thorium enriched solids ($x < 0.4$), a drastic change was observed in the case of uranium enriched samples ($x > 0.5$) which were found to behave like UO_2. A thorium enrichment was also observed at the surface of the solid, indicating the formation of a protective layer of hydrated thorium oxide or hydroxide.[19]

Furthermore, we have recently reported the dissolution of powdered samples of CeO_2 and $Ce_{1-x}Nd_xO_{2-x/2}$ solid solutions by varying several physicochemical properties including crystallization state, reactive surface area, porosity, ...[30] First, the chemical durability of $Ce_{1-x}Nd_xO_{2-x/2}$ was strongly affected by the incorporation of trivalent element in the fluorite structure (as instance, the normalized dissolution rate was increased by a factor of 50 between pure CeO_2 and $Ce_{0.84}Nd_{0.16}O_{1.92}$ during leaching tests in 2 M HNO_3 at 60 °C).[30] While the partial order related to the proton activity or the activation energy indicated that the dissolution was mainly driven by surface reactions occurring at the solid−liquid interface, the chemical durability of $Ce_{1-x}Nd_xO_{2-x/2}$ was also strongly affected by the M(IV)/M(III) ratio due to the presence of oxygen vacancies induced by the M(IV)/M(III) substitution. Finally, the initial normalized dissolution rates were also found to slightly depend on the crystallization state of the powders due to the presence of crystal defects.

2.2. Definitions and Normalization. The comparison of the chemical durability materials with various physicochemical properties requires the normalization either by the reactive surface S (m^2) of the leached samples and by its weight stoichiometric ratio (f_i, expressed as the ratio between the mass of the considered element and the overall mass of the sample). In this objective, normalized weight losses (N_L, also called normalized leachings and expressed in $g \cdot m^{-2}$) were calculated from the concentrations of studied elements,[31] following the equation:

$$N_L(i) = \frac{m_i}{f_i \times S} \quad (1)$$

where m_i (expressed in g) corresponds to the total amount of the element i measured in the solution.

Derivation of eq 1 as a function of leaching time led to the normalized dissolution rate of the element i ($R_L(i)$, expressed in $g \cdot m^{-2} \cdot d^{-1}$) as[30−32]

$$R_L(i) = \frac{dN_L(i)}{dt} = \frac{1}{f_i \times S} \times \frac{dm_i}{dt} = \frac{d}{dt}\left(\frac{C_i \times V \times M_i}{f_i \times S}\right) \approx \frac{V \times M_i}{f_i \times S} \times \frac{dC_i}{dt} \quad (2)$$

where C_i is the concentration of the element in the leachate ($mol \cdot L^{-1}$), V is the volume of leachate (L), f_i is the weight fraction of the element considered in the solid (dimensionless) and M_i its molar mass ($g \cdot mol^{-1}$), and S is the reactive surface of the solid (m^2).

Thereafter, the reaction of dissolution was considered to be congruent when all the normalized dissolution rates were identical (i.e., when all the elements were released with the same ratios than the stoichiometry of the initial material or more generally for $1/3 < R_i/R_j < 3$).[33,34] In the opposite, it was called to be incongruent if at least one element was precipitated as neoformed phases in the back-end of the initial reaction of dissolution.

In this expression, the stoichiometric ratio was assumed to remain almost constant during the leaching tests. This assumption was supported by the strong refractory character of powdered ThO_2,[13] CeO_2,[28,29] and associated $Th_{1-x}Ce_xO_2$ solid solutions and by the associated very low normalized dissolution rates determined, as reported in the following sections. In these conditions, that is, $R_L \approx 10^{-5}$ $g \cdot m^{-2} \cdot d^{-1}$, less than 1% of the initial material would be dissolved after 100 days of leaching.

Moreover, to avoid the initial pulse in the elemental releases usually associated to the presence of crystal defects, nonstoichiometric minor phases, small particles, ... and observed during the first days of leaching tests, the samples were first washed for 3 days in 2 M HNO_3 at room temperature, before the beginning of the dissolution experiments.[31,34,35]

Many authors demonstrated the role of acidity and temperature on the behavior of the materials during dissolution. For a large variety of minerals,[18,19,32,34−44] the dependence of the normalized dissolution rate R_L with the proton activity (for pH < 7) and with

dx.doi.org/10.1021/ic201699t |Inorg. Chem. 2011, 50, 11702–11714

Table 1. Partial Order Related to the Proton Activity and Activation Energy Obtained during the Dissolution of Oxide-Based Materials

mineral/material	partial order n	ref	E_A (kJ·mol^{-1})	ref
CeO_2	0.63 ± 0.05	30	36	30
$Ce_{0.91}Nd_{0.09}O_{1.955}$	1.10 ± 0.10	30	37	30
ThO_2	0.26 ± 0.05	19		
	0.41 ± 0.05	18	20 ± 3	18
UO_2	0.91 ± 0.09	19		
	0.53	48	35 ± 3	49
$Th_{0.63}U_{0.37}O_2$	0.30 ± 0.01	19		
	0.55 ± 0.10	18	33 ± 4	18
$Th_{0.87}Pu_{0.13}O_2$	0.50 ± 0.06	20	ND[a]	
$U_{0.75}Pu_{0.25}O_2$	1.7	26	10−32	26

[a] ND: Not Determined.

temperature was described by the following equation:

$$R_L = k_T' \times (H_3O^+)^n = k_T' \times (\gamma_{H_3O^+} \times [H_3O^+])^n = k'' \times (H_3O^+)^n \times e^{-E_A/RT} \quad (3)$$

In this expression, R_L refers to the proton-promoted normalized dissolution rate, k_T' (expressed in g·m^{-2}·d^{-1}) represents the apparent normalized dissolution rate constant at $-\log(H_3O^+) = 0$. k_T' is independent of the leachate acidity but temperature dependent. k'' is the normalized dissolution rate constant independent of temperature (expressed in g·m^{-2}·d^{-1}). E_A corresponds to the apparent activation energy of the dissolution of the mineral (expressed in kJ·mol^{-1}). It was usually determined from the variation of $\ln(R_L)$ versus the reciprocal temperature.

Because of the formation of adsorbed species onto the surface of leached materials, the E_A values were usually found to be significantly lower than the energy of the formation of chemical bonds (Table 1). Most of the available theories indicated that the dissolution reaction was controlled by the decomposition of an activated complex involving adsorption of aqueous species onto the surface, reaction of adsorbed species between themselves or with atoms of the surface and desorption of the product species formed at the solid/liquid interface.[45,46] The last step was usually slower and therefore controlled the overall rate of the sample dissolution. All these concepts can be accessed experimentally through the Lasaga's approach,[32] which was used during this work.

The n parameter corresponds to the partial order related to the proton activity, (H_3O^+) is the proton activity and $\gamma_{H_3O^+}$ corresponds to the proton activity coefficient. It was usually determined from the variation of $\log(R_L)$ versus $\log(H_3O^+)$. In this study, $\gamma_{H_3O^+}$ values were calculated according to the simplified Pitzer model.[47] From literature, the obtained partial orders related to protons, n (and to hydroxide ions in basic media) were generally found to be fractional ($0 < n < 1$) for several oxide-based materials suggesting the presence of surface-reactions controlling the material dissolution (Table 1). Some authors argued that the n value was linked to the charge of the central cation while other ones contested this hypothesis.[43] Some others suggested that this partial order was directly connected to the number of protons adsorbed onto the surface of the leached samples and thus to the concentration of active sites at the solid/liquid interface.

Table 2. Results of TGA/DTA Experiments for Fluorite-Type $Th_{1-x}Ce_xO_2$ Solid Solutions

cerium mole loading	T (full dehydration)	T (full oxalate decomposition)
$x = 0$	335 °C	570 °C
$x = 0.19$	300 °C	450 °C
$x = 0.72$	220 °C	365 °C
$x = 0.82$	200 °C	370 °C
$x = 1$	190 °C	330 °C

3. EXPERIMENTAL SECTION

3.1. Preparation of Thorium−Cerium Dioxide Solid Solutions. Commercial products from VWR, Sigma-Aldrich, and Strem Chemicals (≥99.9% purity) were used to obtain aqueous solutions of 0.32 ± 0.01 M (Ce) in 0.5 M HNO_3 and of 0.32 ± 0.01 M (Th) in 1 M HNO_3.[50] The initial oxalate precursors were obtained by adding large excess of oxalic acid at room temperature, under stirring, to mixtures of Ce (III) and Th (IV) solutions. The freshly prepared oxalate precipitates were washed several times with deionized water, filtered, and then dried overnight in an oven (90 °C). Depending on the chemical composition considered, XRD patterns revealed that the samples prepared were composed by mixtures of $Th(C_2O_4)_2·2H_2O$. Two H_2O (monoclinic structure, space group $C2/c$),[51] amorphous cerium-(III) oxalate hydrate $Ce_2(C_2O_4)_3·nH_2O$[52,53] and Th−Ce oxalate hydrate solid solution (hexagonal structure, space group $P63/mmc$).[54,55] The quantitative precipitation of the cations (recovery yields higher than 99.9%) thus occurred immediately according to a combination of proposed chemical reactions:

$$(2-2x)Th^{4+} + 2xCe^{3+} + (4-x)H_2C_2O_4 + (4-4x+nx)H_2O \rightarrow (2-2x)Th(C_2O_4)_2·2H_2O\downarrow + xCe_2(C_2O_4)_3·nH_2O\downarrow + (8-2x)H^+ \quad (4)$$

and

$$(2-2x)Th^{4+} + 2xCe^{3+} + 4H_2C_2O_4 + (2+n)H_2O \rightarrow (H_3O)_{2x}Th_{2-2x}Ce_{2x}(C_2O_4)_4·nH_2O\downarrow + (4-2x)H_3O^+ \quad (5)$$

The chemical transformation of oxalate precursors into $Th_{1-x}Ce_xO_2$ solid solutions was also monitored through ThermoGravimetric Analyses (TGA) and Differential Thermal Analyses (DTA), performed on a Setsys Evolution apparatus provided by Setaram. Such experiments were performed in air, with a constant heating rate of 5 °C·min^{-1} up to 300−1000 °C, identical to that applied for the preparation of the final oxides (Table 2, TGA/DTA curves supplied as Supporting Information). As already described for $Th(C_2O_4)_2·2H_2O$,[15,16,56] the full dehydration of the thorium−cerium oxalate hydrates occurred between 190 and 335 °C in several steps depending on the chemical composition of the starting precursors. Moreover, their full conversion to $Th_{1-x}Ce_xO_2$ solid solutions was achieved between 330 °C ($x = 1$) and 570 °C ($x = 0$). The associated DTA peak varied from about 300 °C (cerium end-member and $x = 0.82$) to 325 °C ($x = 0.72$) and 378 °C ($x = 0.19$) to finally reach 390 °C (thorium end-member). This temperature range was higher than that mentioned for other cerium-based oxalate compounds ($Ce_2(C_2O_4)_3·10H_2O$ and $Ce_{2-2x}Nd_{2x}(C_2O_4)_3·10H_2O$[11,30,57,58]) but consistent with that reported for $Th(C_2O_4)_2·2H_2O$[15,16,56] or during the preparation of $Th_{1-x}Ce_xO_2$ solid solutions from $Th_{1-x}Ce_x(OH)_4$ precursors ($T \approx 500$ °C).[12]

dx.doi.org/10.1021/ic201699t |Inorg. Chem. 2011, 50, 11702–11714

$Th_{1-x}Ce_xO_2$ solid solutions were thus obtained above 400 °C according to the following chemical reactions:

$$(2-2x)Th(C_2O_4)_2\cdot 2H_2O + xCe_2(C_2O_4)_3\cdot nH_2O \xrightarrow{\Delta} 2Th_{1-x}Ce_xO_2 + 4CO\uparrow + (4-2x)CO_2\uparrow + (4-4x+nx)H_2O\uparrow \quad (6)$$

and

$$(H_3O)_{2x}Th_{2-2x}Ce_{2x}(C_2O_4)_4\cdot nH_2O + \frac{1}{2}xO_2 \xrightarrow{\Delta} 2Th_{1-x}Ce_xO_2 + 4CO\uparrow + 4CO_2\uparrow + (3x+n)H_2O \quad (7)$$

This chemical transformation was associated to the strong change in the powder color from white to yellow because of the oxidation of cerium(III) into cerium(IV) during the heating treatment.

3.2. Characterization. *3.2.1. X-ray Powder Diffraction.* XRD patterns were collected between 10 and 80° ($\theta-2\theta$ mode) using a Bruker D8 Advance X-ray diffractometer (Cu $K\alpha_{1,2}$ radiation, λ = 1.5418 Å) equipped with a linear Lynx-eye detector. For all the powdered samples, a step of 0.01° and a counting time of 1.5 s·step^{-1} were considered. The unit cell parameters for fluorite-type $Th_{1-x}Ce_xO_2$ dioxides were refined by the Rietveld method using the Thomson-Cox-Hastings Pseudo Voigt convoluted with an axial divergence asymmetry function[59] available in the Fullprof_Suite program.[60] Pure silicon was used to extract the instrumental functions.

3.2.2. ESEM. In situ high temperature environmental scanning electron microscopy (HT-ESEM) experiments were performed using a field emission gun environmental scanning electron microscope (model FEI QUANTA 200 ESEM FEG) equipped with a 1500 °C hot stage. The sample was directly placed in a 5 mm diameter MgO crucible covered with platinum paint then heated up to 1000 °C in the ESEM chamber with a rate of 20 °C·min^{-1}. Micrographs were recorded each 100 °C during the heating treatment of the sample with various magnifications. The furnace temperature was controlled by a thermocouple placed near the MgO crucible. The observations were performed in air atmosphere at an operating pressure of 120 Pa. A specific detector was used for in situ gaseous secondary electron imaging at high temperature.

The chemical composition of the powders was determined by Energy Dispersive Spectrometry (EDS) coupled with the ESEM device. Samples were carbon-coated polished preparation of powders embedded in epoxy. The final analysis was the average of 12 measurements (40000 counts, 11.4 nm working distance, 15 kV acceleration voltage) considering the L series for cerium and the M series for thorium. Oxygen content was determined by difference. With those conditions, the absolute accuracy for x_{Ce} was assumed to be ±0.01.

3.2.3. Specific Surface Area and Porosity Distribution. The specific surface area measurements were performed with a Micromeritics ASAP 2020 apparatus using nitrogen adsorption (Brunauer, Emmet and Teller, BET method) at 77 K. The pore size distribution of the oxide samples was determined from the desorption branches of nitrogen adsorption isotherm according to the BJH (Barret, Joyner and Halenda) method, based on the Kelvin equation, which links the pore size with critical condensation pressure, by assuming a straight cylindrical pore model.[61] Prior to the measurements, the samples were dried at 300 °C for 3 h to ensure their complete outgassing.

3.3. Leaching Experiments. Leaching tests were performed using batch experiments in polytetrafluoroethylene containers at room temperature. 100 to 150 mg of powder were put in contact with 25 mL of 0.1−6 M HNO_3 for few weeks to several months. An aliquot of 700 μL was regularly taken off then renewed corresponding to less than 3% of the total volume. After centrifugation at 12000 rpm (to avoid the presence of colloids smaller than 11 nm[62]), the thorium and cerium concentrations were determined by inductively-coupled plasma atomic emission spectroscopy (ICP-AES, Spectro Arcos). The intensity of the peaks was recorded at λ = 448.691, 418.660, 413.765, and 413.380 nm for cerium and at λ = 401.913, 283.730, 283.231, and 274.716 nm for thorium to avoid any interference between the studied elements. The 0.5 M HNO_3 solution used for dilution of samples was considered as blank reference.

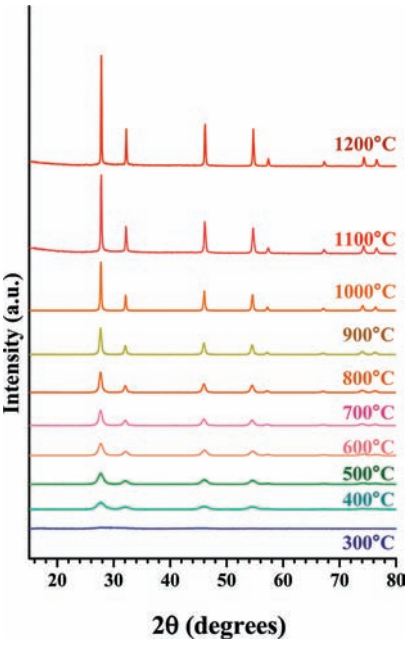

Figure 1. XRD patterns of $Th_{0.81}Ce_{0.19}O_2$ recorded after heating the samples at various temperatures between 300 and 1200 °C (air, 2 h).

4. RESULTS AND DISCUSSION

4.1. Structural and Microstructural Characterization. *4.1.1. Chemical Composition Determination and XRD Characterization.* The variation of the XRD patterns of $Th_{0.81}Ce_{0.19}O_2$ versus heating temperature (300 °C < T < 1200 °C) is reported as an example in Figure 1. At 300 °C, XRD patterns did not evidence any XRD lines, showing that the sample was fully amorphous. This observation was correlated to the complete dehydration then to the beginning of the decomposition of the oxalate precursors that agreed well with the data reported by Balboul et al. on amorphous $Nd_2(C_2O_4)_3$[63] and by Dash et al. on $Th(C_2O_4)_2\cdot 2H_2O$.[64] The $Th_{1-x}Ce_xO_2$ crystallization started at 400 °C. This temperature was significantly higher than that mentioned in literature by Yildiz ($T \approx$ 200 °C) when performing the preparation of $Th_{1-x}Ce_xO_2$ nanopowders by conversion of $Th_{1-x}Ce_x(OH)_4$ precipitates.[12] Such difference was assigned to the higher temperature required for the full decomposition of oxalates and to the nanometric character of the hydroxide precursors used during their study.[12] Above 400 °C, all the XRD lines characteristic of the fluorite-type structure (space group $Fm\bar{3}m$) adopted by ThO_2 (JCPDS file 00−042−1462) and CeO_2 (JCPDS file 01−081−0792) were observed.[13,65] No additional phase was detected which agreed well with the formation of $Th_{1-x}Ce_xO_2$ solid solutions.[4,6,11] From 400 to 800 °C, the XRD lines remained broad and indicated that the crystallization state was not optimal. Conversely, it was clearly improved above 800 °C.

The XRD diagram was refined by Rietveld method considering a $Fm\bar{3}m$ fluorite type $Th_{1-x}Ce_xO_2$ solid solution (see data supplied as Supporting Information for $Th_{0.81}Ce_{0.19}O_2$). The comparison between the calculated XRD patterns by Rietveld program revealed a good agreement with the experimental data.

dx.doi.org/10.1021/ic201699t |Inorg. Chem. 2011, 50, 11702–11714

The refined unit cell parameter determined confirmed the formation of $Th_{1-x}Ce_xO_2$ solid solution instead of a two fluorite-type dioxide mixture. Moreover, the chemical compositions determined by interpolation from unit-cell parameters of homemade ThO_2 and CeO_2 agreed well with chemical compositions determined by X-EDS (Table 3). The unit cell parameter decreased linearly when increasing the cerium mole loading in the solid in good agreement with the replacement of thorium ($^{VIII}r(Th^{4+})$ = 1.05 Å[66]) by the smaller tetravalent cerium ($^{VIII}r(Ce^{4+})$ = 0.96 Å[66]) in $Th_{1-x}Ce_xO_2$ solid solutions, according to the Vegard's law (see variation of unit cell parameters reported as Supporting Information).

Table 3. Expected and Experimental Compositions (X-EDS, XRD) of Fluorite-Type $Th_{1-x}Ce_xO_2$ Prepared after Heating at 1000°C and Associated Refined Unit Cell Parameters

expected chemical formula ($Th_{1-x}Ce_xO_2$)	x (exp.) (from EDS)	unit cell parameters (Å)	x (exp.) (from XRD) [a]
x = 0	0	a = 5.5971(1)	0
x = 0.10	0.06 ± 0.01	a = 5.585(1)	0.06
x = 0.20	0.19 ± 0.03	a = 5.5702(1)	0.19
x = 0.30	0.31 ± 0.04	a = 5.5329(1)	0.36
x = 0.50	0.55 ± 0.03	a = 5.5044(1)	0.50
x = 0.60	0.58 ± 0.03	a = 5.4942(1)	0.55
x = 0.70	0.72 ± 0.01	a = 5.4725(1)	0.67
x = 0.80	0.82 ± 0.01	a = 5.4466(1)	0.81
x = 0.90	0.91 ± 0.01	a = 5.4302(1)	0.89
x = 1.0	1	a = 5.4104(1)	1

[a] x values interpolated from unit-cell parameters of homemade ThO_2 and CeO_2.

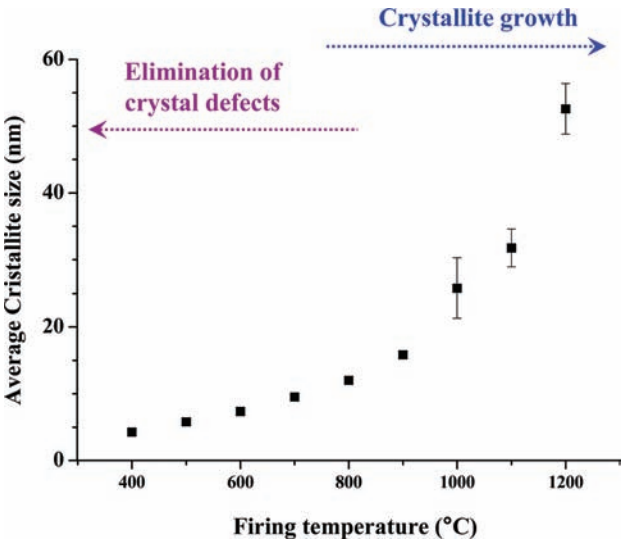

Figure 2. Variation of the average crystallite size versus the firing temperature obtained for $Th_{0.81}Ce_{0.19}O_2$.

The variation of the crystallization state of $Th_{1-x}Ce_xO_2$ solid solutions was monitored in a first approach versus the heating temperature through the average full width at half maximum (fwhm) from the more intense XRD lines. This latter strongly decreased from 400 to 600 °C then progressively stabilized for T > 1000 °C. Above this temperature, the crystallization state of $Th_{1-x}Ce_xO_2$ was considered to be optimized. Furthermore, the Rietveld method allowed confirming this point by determining the size of coherent domains, corresponding to the various crystallization states (Figure 2). The average crystallite size increased slightly and continuously from 5 to 15 nm between 400 and 900 °C then more rapidly above this temperature to finally reach about 50−60 nm at 1200 °C. This observation suggested the first elimination of crystal defects and amorphous domains (T < 900 °C) leading to the improvement of the crystallization state of the solid with a limited growth of the coherent domains. It was then followed by the crystallites growth for $T \geq$ 900 °C through Ostwald ripening process[67,68] almost similar to that responsible for sintering processes at the grain scale. The activation energy for the crystallite growth of $Th_{1-x}Ce_xO_2$, $E_{A,CG}$, estimated from the variation of the logarithm of the crystallite size versus the reciprocal temperature according an Arrhenius's law[69] for $T \geq$ 900 °C (see Supporting Information), reached 21 ± 3 kJ.mol^{-1}. This value was consistent with that recently reported for nanopowdered CeO_2 ($E_{A,CG}$ = 17 kJ.mol^{-1})[70] and $Ce_{1-x}Nd_xO_{2-x/2}$ solid solutions ($E_{A,CG}$ = 21 ± 2 kJ·mol^{-1}).[30]

4.1.2. Morphological Characterization. The microstructure of the samples prepared was followed versus the heating temperature by in situ HT-ESEM observations (Figure 3). It was coupled with specific surface area (Figure 4A) and porosity (Figure 4B) measurements.

The oxalate to oxide transformation followed in situ by HT-ESEM (Figure 3) showed that the samples were constituted by nanometric grains associated in square aggregates of 3−5 μm in length. As already observed during the preparation of ceria

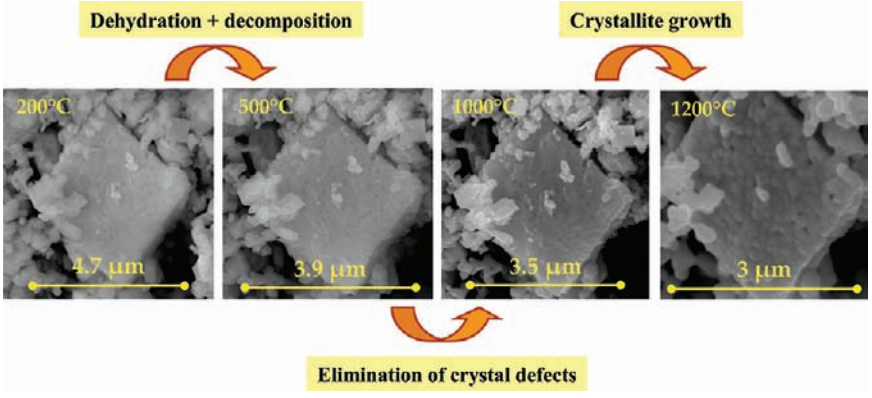

Figure 3. In situ HT-ESEM micrographs collected during the heat treatment of thorium−cerium oxalate precursors at 200, 500, 1000, and 1200 °C (scale bars presented in each micrograph correspond to the square diagonals).

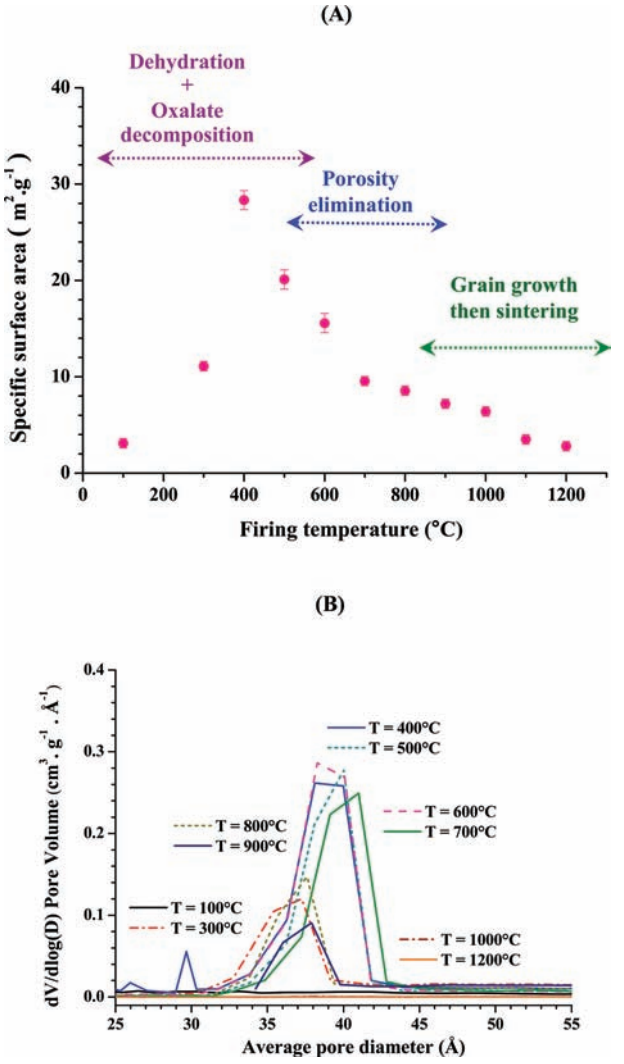

Figure 4. Variations of the specific surface area versus the firing temperature (t = 2 h) observed for $Th_{0.81}Ce_{0.19}O_2$ (A) and of the incremental pore area versus the average pore diameter (B).

from cerium oxalate, this morphology was kept all during the oxalate to oxide conversion. However, the oxalate transformation, i.e. the release of H_2O, CO and CO_2 gaseous molecules was characterized by a contraction of the aggregates size of 17% between 90 and 500 °C. Then, the grain size slightly decreased correlatively to the crystallite growth and to the beginning of the sintering process.

However, these pictures did not explain the strong variations of surface area between 200 and 800 °C mainly because the pores (average size of 3.5−4.5 nm) were not big enough to be highlighted unambiguously. The grain contraction continued when increasing temperature up to 1200 °C. At this holding temperature, the microstructure of the grains was modified since some grains boundaries and bridges were clearly observed within the agglomerates, as a proof of the grain growth process.

The specific surface area of the raw powder was equal to 3 $m^2 \cdot g^{-1}$ (Figure 4A). It significantly increased by almost one decade when heating the samples up to 300 or 400 °C (S_{BET} = 11 and 28 $m^2 \cdot g^{-1}$ for T = 300 and 400 °C, respectively) as already reported during the conversion of $Th_{1-x}U_x(C_2O_4)_2 \cdot 2H_2O$,[16] $Ce_2(C_2O_4)_3 \cdot 10H_2O$,[11,71] $Ce_{2-2x}Nd_{2x}(C_2O_4)_3 \cdot 10H_2O$,[30] and $Th_{1-x}Ce_x(C_2O_4)_2 \cdot nH_2O$.[11] This phenomenon was mainly assigned to the dehydration of the samples and to the decomposition of the oxalate entities into CO and CO_2, which induced the formation of defects (cracks, pores, ...) within the material. These results were consistent with the temperature range expected from TGA and DTA experiments (220−460 °C) and to the observation of poorly crystallized samples from XRD.

Above this temperature, the specific surface area progressively decreased simultaneously to the improvement of the crystallization state of the samples then to the crystallite growth. Simultaneously, the powder morphology was almost preserved through an isomorphic transformation despite such great variations in the specific surface area. For this reason, porosity modifications were examined in connection with the release of gaseous molecules during the oxalate conversion. Desorption isotherm analysis of $Th_{1-x}Ce_xO_2$ solid solutions with the BJH method were thus performed to give additional information on the pore size distribution (Figure 4B). This study confirmed that the mesoporosity remained very low in the starting material. It significantly increased when heating the samples between 400 and 700 °C mainly because of the release of H_2O, CO, and CO_2 gaseous molecules. At these heating temperatures, the mesoporosity contributed to 62 to 75% of the developed specific surface area. This contribution significantly decreased at 800 °C then 900 °C with associated contributions to 58% and 40% of S_{BET}, respectively. Finally, such mesoporosity disappeared above 1000 °C simultaneously to the crystallite growth.

The complete characterization of the samples showed that a large panel of $Th_{1-x}Ce_xO_2$ samples was obtained from the complete conversion of oxalate precursors above 400 °C. From X-EDS and XRD, all exhibited the expected chemical composition while the variation of several properties of interest (crystallite size, specific surface area, mesoporosity) was monitored. Their effect on the chemical durability was then studied.

4.2. Dissolution of $Th_{1-x}Ce_xO_2$ Samples. The variation of the normalized weight losses, N_L(Th) and N_L(Ce) determined when leaching $Th_{0.81}Ce_{0.19}O_2$ samples (initially fired at 600, 800, 1000, or 1200 °C) in 2 M HNO_3 at 60 °C and using static conditions is presented in Figure 5. The general evolution of N_L versus the leaching time clearly exhibited two tendencies. The first one, that is kinetically controlled, was observed before at least 20 days of leaching time. This linear variation allowed the determination of the initial normalized dissolution rates. It was often followed by a slope drop which was usually assumed to result from the establishment of thermodynamic controlled phenomena, allowing the determination of the normalized dissolution rates near the establishment of saturation processes. Moreover, as it was expected considering the results already reported on cerium and neodymium based compounds,[30] the higher the heating temperature, the slower the normalized dissolution rate, as a consequence of the improvement of the powder crystallization state (see following sections).

The direct comparison of the normalized dissolution rates $R_{L,0}$(Th) and $R_{L,0}$(Ce) also traduced some discrepancies in the element releases. It was underlined by plotting the variation of the congruence ratio $r = R_{L,0}(Ce)/R_{L,0}(Th)$ versus the heating temperature of the samples (Figure 6). Both elements were released with almost the same normalized dissolution rates (i.e., r = 1) for firing temperatures ranging between 400 and 800 °C, suggesting the congruent nature of the dissolution of $Th_{0.81}Ce_{0.19}O_2$. On the contrary, cerium was found to be preferentially released above these heating temperatures. As clearly observed in this figure for

dx.doi.org/10.1021/ic201699t |Inorg. Chem. 2011, 50, 11702–11714

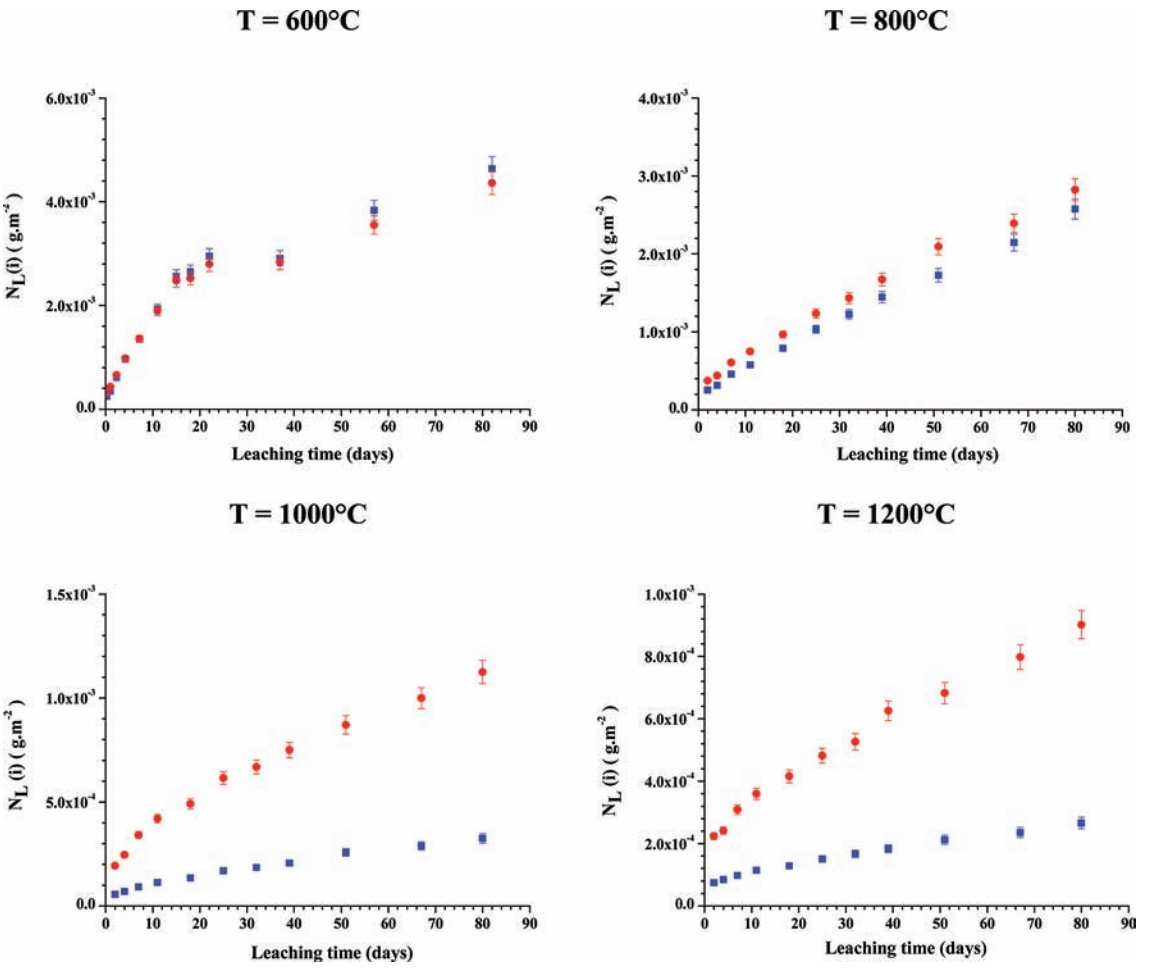

Figure 5. Evolution of the normalized leachings N_L(Th) (blue) and N_L(Ce) (red) obtained during leaching tests (2 M HNO_3, T = 60 °C) of $Th_{0.81}Ce_{0.19}O_2$ samples fired at 600, 800, 1000, and 1200 °C.

T > 800 °C, the higher the heating temperature, the stronger the differences between both elements. In a first approach, one could assign such effect to steric differences between cerium and thorium. However, the constant behavior of $Th_{1-x}Ce_xO_2$ solid solutions in the whole composition range excluded this assumption (see next section, Figure 7). Several hypotheses were formulated to explain such differences in the chemical behavior of both elements:

- The first probable hypothesis could result from the partial reduction of Ce(IV) to Ce(III), at the extreme surface of the sample, during the heating treatment itself leading to the preferential release of this latter during dissolution tests. This reduction was already mentioned in the literature even though it was found to be lower for $Th_{1-x}Ce_xO_2$ solid solutions than for CeO_{2-x}.[72]
- Also, one could also argue that this effect may be due to the additional specific reduction of Ce(IV) to Ce(III) at the solid/liquid interface during the leaching tests. Indeed, despite the high value of the standard potential of Ce^{IV}/Ce^{III} in solution ($E^0(Ce^{IV}/Ce^{III})$ = 1.44 V/NHE), such reaction could be induced by nitrous acid (HNO_2, $E_0 \approx 1$ V/NHE) formed trough the HNO_3 instability in such experimental conditions (high acid concentrations and T = 60 °C). Indeed, even if the HNO_2 concentration would remain low compared to that of HNO_3 (typically fixed to $\sim 10^{-3}$ M through thermodynamic equilibria involving NO and NO_2), it could be sufficient to reduce Ce(IV) to Ce(III) released at the lower scale (in the μM range) near the solid/solution interface consequently to the sample dissolution.[73]

For both assumptions, since the normalized dissolution rates decreased significantly when increasing the heating temperature of the initial powder (see following sections), this effect was potentially concealed for the higher normalized dissolution rates (i.e., for the lower firing temperatures) then clearly underlined for the higher heating temperatures (i.e., slower R_L values).

Even if the difference between both elements was limited ($1 < r < 3.6$), it resulted for both hypotheses from the existence of redox reactions involving tetravalent cerium. From these data, it was thus possible to separate the dissolution of the fluorite-type ceramic itself from the contribution of redox reactions occurring at the solid/liquid interface. Since thorium was not significantly affected by this effect, it was preferentially used as a tracer for the establishment of the multiparametric expression of the normalization dissolution rate of $Th_{1-x}Ce_xO_2$ solid solutions.

4.2.1. Influence of Composition. The effect of chemical composition on the dissolution of $Th_{1-x}Ce_xO_2$ solid solutions was examined in 2 M HNO_3 at 60 °C. The variation of the initial normalized dissolution rates $R_{L,0}$(Th) and $R_{L,0}$(Ce) versus the cerium mole loading is plotted in Figure 7, while the corresponding data is supplied as Supporting Information. From these results, it clearly

dx.doi.org/10.1021/ic201699t |*Inorg. Chem.* 2011, 50, 11702–11714

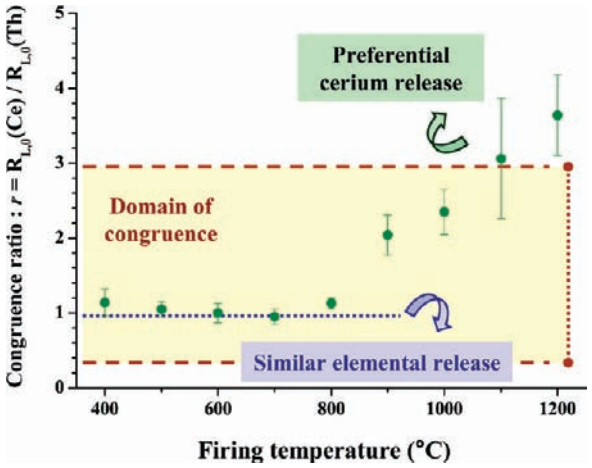

Figure 6. Variation of the congruence ratio $r = R_{L,0}(Ce)/R_{L,0}(Th)$ obtained during leaching tests (2 M HNO_3, $T = 60$ °C) of $Th_{0.81}Ce_{0.19}O_2$ versus the firing temperature showing the congruence dissolution for $T \leq 800$ °C and the preferential cerium release for $T > 900$ °C.

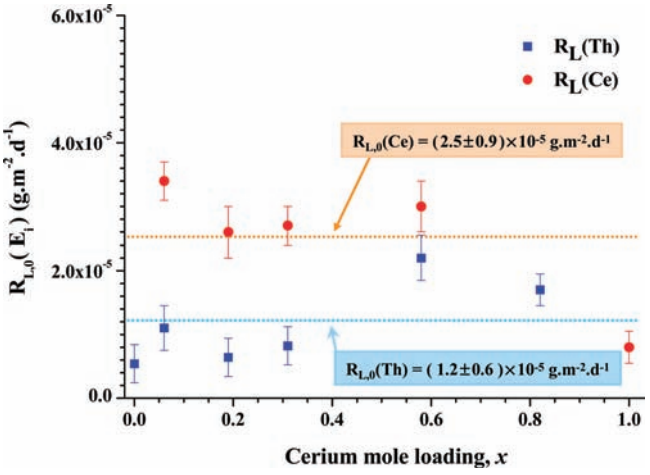

Figure 7. Variation of $R_{L,0}$ (Th) and $R_{L,0}$ (Ce) versus the cerium mole loading, x during leaching tests of $Th_{1-x}Ce_xO_2$ solid solutions in 2 M HNO_3 at $T = 60$ °C (firing temperature of the samples 1000 °C).

appeared that, conversely to that was observed for $Th_{1-x}U_xO_2$ and $Ce_{1-x}Nd_xO_{2-x/2}$, the chemical durability of $Th_{1-x}Ce_xO_2$ solid solutions remained almost constant in the whole composition range. Moreover, the average initial normalized dissolution rates reached $R_{L,0}(Th) = (1.2 \pm 0.6) \times 10^{-5}$ g·m^{-2}·d^{-1} and $R_{L,0}(Ce) = (2.5 \pm 0.9) \times 10^{-5}$ g·m^{-2}·d^{-1} (Figure 7). This slight difference between both values also confirmed the results presented in Figure 6 when leaching $Th_{0.81}Ce_{0.19}O_2$ powdered samples prepared at various temperatures. The chemical durability of such solid solutions then should be less sensitive to potential heterogeneities in the Th/Ce distribution (including that coming from the synthesis method) than other fluorite-type solid-solutions, such as $Th_{1-x}U_xO_2$[15,16] or $Ce_{1-x}Nd_xO_{2-x/2}$.[30]

4.2.2. Influence of the Nitric Acid Concentration. $Th_{0.81}Ce_{0.19}O_2$ powdered samples were leached in various nitric acid concentrations (0.1, 0.5, 2, 4, and 6 M HNO_3, Figure 8A). The associated free proton concentrations were determined according to literature.[74,75] The initial normalized dissolution rates $R_{L,0}(Th)$ are gathered in

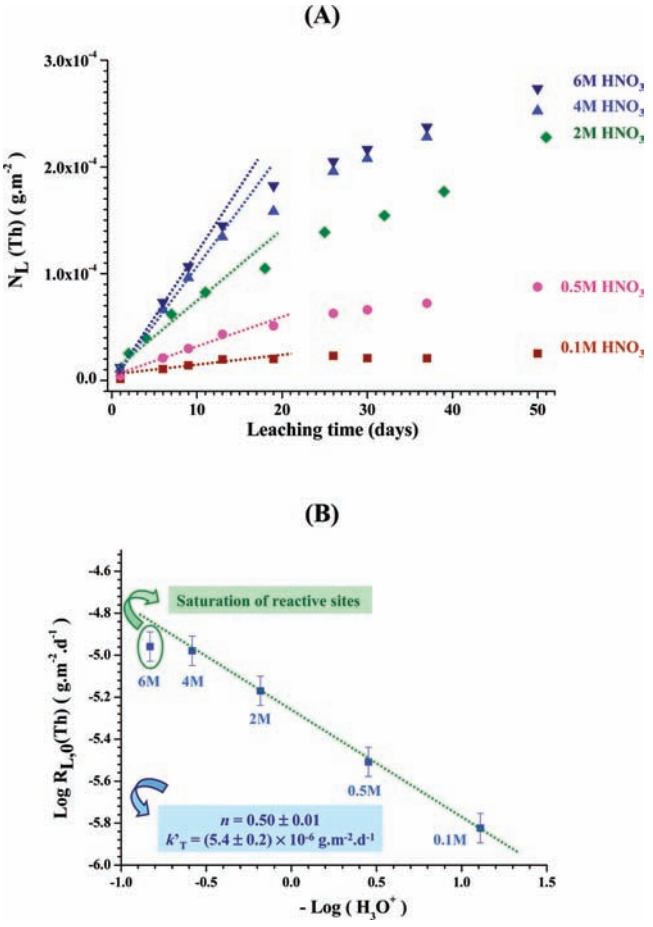

Figure 8. Evolution of the normalized leaching $N_L(Th)$ during leaching tests of $Th_{0.81}Ce_{0.19}O_2$ at 60 °C in various nitric acid solutions (A): 6 M HNO_3 (purple), 4 M HNO_3 (blue), 2 M HNO_3 (green), 0.5 M HNO_3 (magenta), and 0.1 M HNO_3 (red) and variation of log ($R_{L,0}$(Th)) versus the opposite log (H_3O^+) (B).

Table 4 while the variation of log ($R_{L,0}$(Th)) versus the leachate acidity is plotted in Figure 8B for $Th_{0.81}Ce_{0.19}O_2$ (on a sample fired at 1000 °C). For all the studied media, the normalized dissolution rates obtained during leaching tests performed at 60 °C were very slow: from $R_{L,0}(Th) = (1.5 \pm 0.2) \times 10^{-6}$ g·m^{-2}·d^{-1} obtained in 10^{-1} M HNO_3 up to $R_{L,0}(Th) = (1.1 \pm 0.1) \times 10^{-5}$ g·m^{-2}·d^{-1} in 6 M HNO_3. All these values confirmed the high chemical durability already described for both dioxide end-members: ThO_2 ($R_{L,0}(Th) = (1.7 \pm 0.1) \times 10^{-7}$ g·m^2·d^{-1} when leaching the samples in 5 M HNO_3 at $T = 25$ °C)[13,18] and CeO_2 ($R_{L,0}(Ce) = (1.0 \pm 0.3) \times 10^{-5}$ g·m^2·d^{-1} when leaching the samples in 2 M HNO_3 at $T = 60$ °C).[28,29] Moreover, the nitric acid concentration significantly affected the behavior of the samples as already described for ThO_2, $Th_{1-x}U_xO_2$, and $Ce_{1-x}Nd_xO_{2-x/2}$ samples.[18,19,30]

Indeed, an increase of 1 order of magnitude was obtained between 10^{-1} and 4 M HNO_3 for $Th_{0.81}Ce_{0.19}O_2$ ($R_{L,0}(Th) = (1.5 \pm 0.2) \times 10^{-6}$ and $(1.0 \pm 0.3) \times 10^{-5}$ g·m^{-2}·d^{-1}, respectively), which was in good agreement with that reported for pure CeO_2.[30] As suggested by the Lasaga's approach,[32] the normalized dissolution rate increased linearly with the logarithm of the proton concentration between 0.1 M HNO_3 and 4 M HNO_3. Conversely, the influence of nitric acid concentration decreased for 6 M HNO_3 (Figure 8) probably because of the

dx.doi.org/10.1021/ic201699t |Inorg. Chem. 2011, 50, 11702–11714

Table 4. Initial Normalized Dissolution Rates $R_{L,0}(Th)$ ($g \cdot m^{-2} \cdot d^{-1}$) Obtained during Leaching Tests of $Th_{0.81}Ce_{0.19}O_2$ (Fired at 1000°C) Performed at 60°C in Various Nitric Acid Leaching Solutions

HNO_3 concentration	0.1 M	0.5 M	2 M	4 M	6 M
$R_{L,0}$ (Th)	$(1.5 \pm 0.2) \times 10^{-6}$	$(3.1 \pm 0.1) \times 10^{-6}$	$(6.4 \pm 1.0) \times 10^{-6}$	$(1.0 \pm 0.3) \times 10^{-5}$	$(1.1 \pm 0.1) \times 10^{-5}$

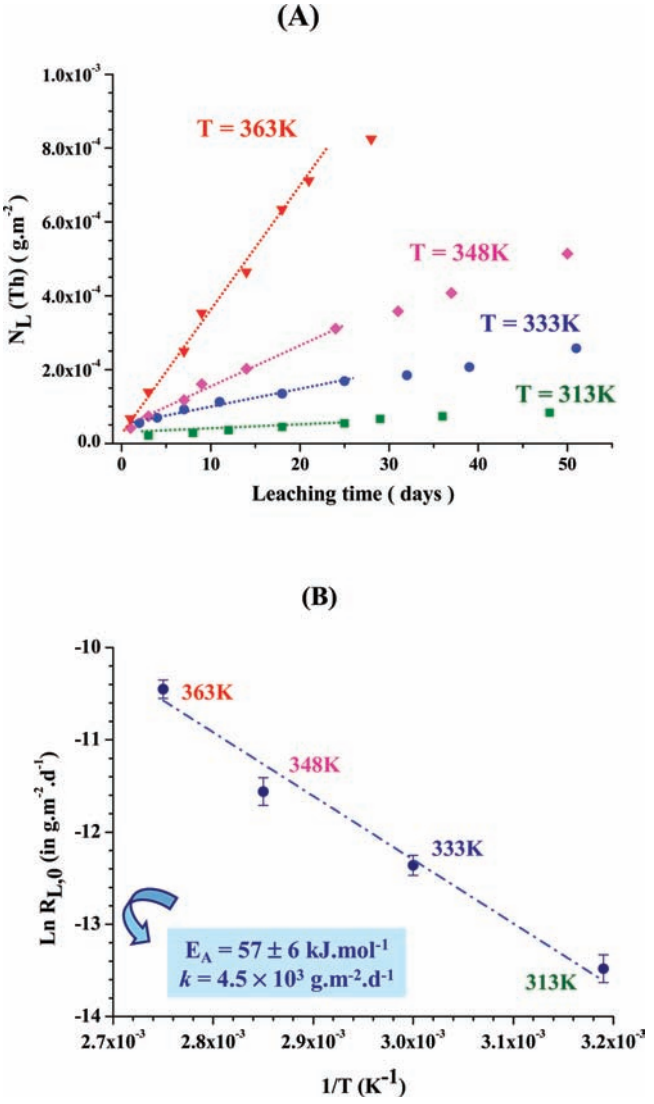

Figure 9. Evolution of log (N_L(Th)) for several leaching temperatures and associated variation of Ln ($R_{L,0}$(Th)) versus the reciprocal leaching temperature during leaching tests of $Th_{0.81}Ce_{0.19}O_2$ (2 M HNO_3).

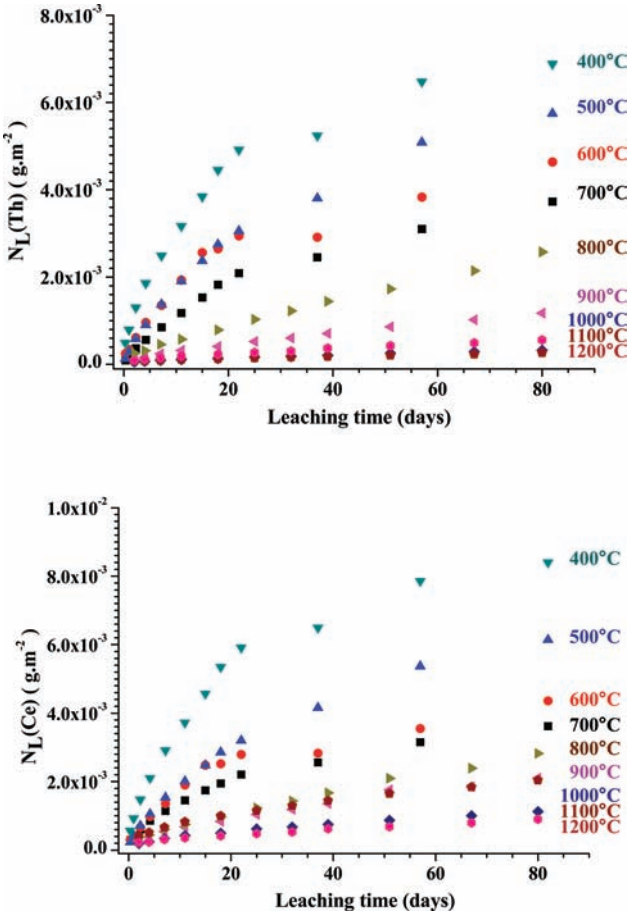

Figure 10. Evolution of the normalized leachings N_L(Th) and N_L(Ce) obtained during the dissolution of powdered $Th_{0.81}Ce_{0.19}O_2$ samples (2 M HNO_3, T = 60 °C) prepared for various temperatures of heating treatment: 400 °C (green), 500 °C (blue), 600 °C (red), 700 °C (black), 800 °C (olive green), 900 °C (magenta), 1000 °C (purple), 1100 °C (burgundy), and 1200 °C (hot pink).

progressive saturation of active surface sites that reduced significantly the effect of protons in this concentration range.

The linear regression obtained from the variation of log ($R_{L,0}$(Th)) versus log (H_3O^+) (eq 3) led to log (k_T') = −5.27 ± 0.02 while n reached 0.50 ± 0.01. Such a value suggested the existence of surface reactions occurring at the solid/liquid interface and involving the adsorption of active species at the interface prior the dissolution of the solid, as described in the Lasaga's approach.[32] Moreover, it was consistent with that reported for several other materials and minerals (Table 1) including refractory ThO_2 (n = 0.41 ± 0.05) and CeO_2 (n = 0.63 ± 0.05). This n value thus should not be affected by the chemical composition of the leached samples conversely to that observed for $Th_{1-x}U_xO_2$ solid solutions. This difference could result from the strong oxidation of U(IV) to UO_2^{2+} in nitric acid solutions compared to the weak reduction of Ce(IV) to Ce(III).[18,19]

4.2.3. Influence of the Temperature. As already discussed, temperature is also a key parameter affecting the behavior of the samples during dissolution. The evolution of N_L(Th) versus the leaching time obtained when leaching $Th_{0.81}Ce_{0.19}O_2$ powdered samples is reported in Figure 9A. For the four studied temperatures, the N_L(Th) evolution followed a linear trend leading to accurate values of the normalized dissolution rates $R_{L,0}$(Th). Moreover, the linear variation of ln($R_{L,0}$(Th)) versus the reciprocal leaching temperature (Figure 9B) allowed the determination

dx.doi.org/10.1021/ic201699t |Inorg. Chem. 2011, 50, 11702–11714

Table 5. Initial Normalized Dissolution Rates $R_{L,0}$(Th) and $R_{L,0}$(Ce) and Long-Term Normalized Dissolution Rates $R_{L,t}$(Th) and $R_{L,t}$(Ce) (Expressed in $g \cdot m^{-2} \cdot d^{-1}$) Obtained during the Dissolution of $Th_{0.81}Ce_{0.19}O_2$ for Several Calcination Temperatures (2 M HNO_3, T = 60 °C)

heating temperature	$R_{L,0}$(Th)	$R_{L,0}$(Ce)	$R_{L,t}$(Th)	$R_{L,t}$(Ce)
400 °C	$(2.9 \pm 0.2) \times 10^{-4}$	$(3.3 \pm 0.3) \times 10^{-4}$	$(3.6 \pm 0.3) \times 10^{-5}$	$(4.6 \pm 0.3) \times 10^{-5}$
500 °C	$(2.0 \pm 0.1) \times 10^{-4}$	$(2.1 \pm 0.1) \times 10^{-4}$	$(3.5 \pm 0.4) \times 10^{-5}$	$(4.0 \pm 0.4) \times 10^{-5}$
600 °C	$(1.5 \pm 0.1) \times 10^{-4}$	$(1.5 \pm 0.1) \times 10^{-4}$	$(2.6 \pm 0.3) \times 10^{-5}$	$(2.6 \pm 0.3) \times 10^{-5}$
700 °C	$(9.8 \pm 0.5) \times 10^{-5}$	$(9.3 \pm 0.5) \times 10^{-5}$	$(2.4 \pm 0.2) \times 10^{-5}$	$(2.1 \pm 0.2) \times 10^{-5}$
800 °C	$(3.1 \pm 0.1) \times 10^{-5}$	$(3.5 \pm 0.1) \times 10^{-5}$	ND[a]	ND[a]
900 °C	$(2.2 \pm 0.1) \times 10^{-5}$	$(4.5 \pm 0.4) \times 10^{-5}$	$(1.2 \pm 0.1) \times 10^{-5}$	$(1.9 \pm 0.2) \times 10^{-5}$
1000 °C	$(6.4 \pm 0.4) \times 10^{-6}$	$(1.5 \pm 0.1) \times 10^{-5}$	$(2.9 \pm 0.2) \times 10^{-6}$	$(9.3 \pm 0.2) \times 10^{-6}$
1100 °C	$(1.5 \pm 0.7) \times 10^{-5}$	$(4.6 \pm 0.3) \times 10^{-5}$	$(5.1 \pm 0.3) \times 10^{-6}$	$(1.5 \pm 0.1) \times 10^{-5}$
1200 °C	$(4.4 \pm 0.1) \times 10^{-6}$	$(1.6 \pm 0.2) \times 10^{-5}$	$(2.1 \pm 0.3) \times 10^{-6}$	$(7.4 \pm 0.5) \times 10^{-6}$

[a] ND: Not determined

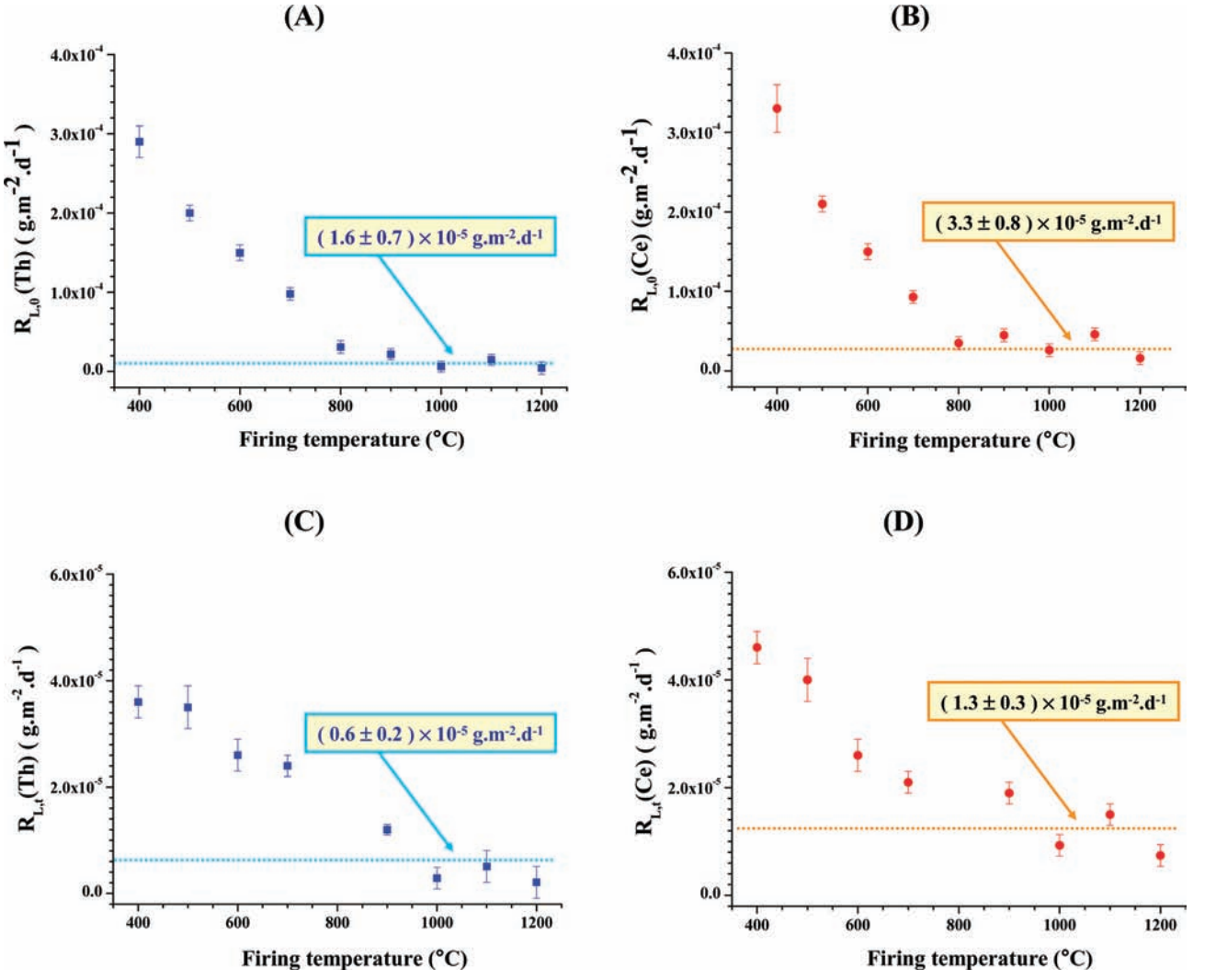

Figure 11. Variation of the initial normalized dissolution rate $R_{L,0}$(Th) and $R_{L,0}$(Ce) (A,B) and of the long-term normalized dissolution rate $R_{L,t}$(Th) and $R_{L,t}$(Ce) (C, D) versus the firing temperature obtained during leaching tests of $Th_{0.81}Ce_{0.19}O_2$ (2 M HNO_3, T = 60 °C).

of an activation energy associated to the dissolution reaction of 57 ± 6 kJ·mol^{-1}.

Once again, the dependence of the normalized dissolution rate on temperature was significant since an increase of one decade was obtained between 40 °C ($R_{L,0}$(Th) = $(1.4 \pm 0.5) \times 10^{-6}$ g·m^{-2}·d^{-1} and 90 °C ($R_{L,0} = (2.9 \pm 0.1) \times 10^{-5}$ g·m^{-2}·d^{-1}). It is worth noting that such values confirmed the control of the dissolution by surface reactions occurring at the solid/

dx.doi.org/10.1021/ic201699t |Inorg. Chem. 2011, 50, 11702–11714

liquid interface as suggested by the Lasaga's approach and as already described in literature for several fluorite-type dioxide compounds.[18,19,30,31] Moreover, they were too high to consider that only diffusion phenomena controlled the dissolution (since $E_A > 20$ kJ·mol^{-1}).[76] Such values were consistent with that obtained for other fluorite-type dioxides like ThO_2, CeO_2, and PuO_2 ($E_A = 20-37$ kJ·mol^{-1}) but significantly lower than that mentioned for $Ce_{1-x}Nd_xO_{2-x/2}$ with large neodymium amounts ($E_A \approx 80$ kJ·mol^{-1}) in which the M(III)/M(IV) substitution clearly affected the variation of the chemical durability with leaching temperature.

4.2.4. Influence of the Crystallization State. The chemical durability of $Th_{0.81}Ce_{0.19}O_2$ samples with various crystallization states was studied in 2 M HNO_3 at 60 °C. The associated evolutions of the normalized weight losses N_L(Th) and N_L(Ce) when leaching powdered samples heated at various temperatures between 400 and 1200 °C are gathered in Figure 10. The associated initial ($R_{L,0}$(Th) and $R_{L,0}$(Ce)) and long-term ($R_{L,t}$(Th) and $R_{L,t}$(Ce)) normalized dissolution rates are gathered in Table 5 while their variations versus the firing temperature are reported in Figure 11.

In spite of the normalization of the elementary releases by the mass ratios (f_i) and by the reactive surface area (S) associated to the solid/liquid interface (see eqs 3 and 4), the initial normalized dissolution rates $R_{L,0}$(Th) and $R_{L,0}$(Ce) were divided by almost a factor of 10 from 400 °C ($R_{L,0}$(Th) = $(2.9 \pm 0.2) \times 10^{-4}$ g·m^{-2}·d^{-1}) down to 800 °C ($R_{L,0}$(Th) = $(3.1 \pm 0.1) \times 10^{-5}$ g·m^{-2}·d^{-1}). Above 800 °C, the normalized dissolution rate values were almost stabilized (Figure 11). This two-step variation with the heating temperature was directly connected to that observed for the crystallite growth. As recently observed for $Ce_{1-x}Nd_xO_{2-x/2}$ solid solutions, the elimination of crystal defects and of amorphous domains (400 °C < T < 800 °C) clearly impacted the $R_{L,0}$ values, showing the role played by the crystallization state. On the contrary, the change in microstructural state (Figure 2, 900 °C < T < 1200 °C) seemed to have no effect on the chemical durability of the leached samples.

The evolution of the normalized dissolution rate exhibited two tendencies for the major part of the experiments performed using static conditions. A significant decrease from the initial normalized dissolution rates, $R_{L,0}(i)$ to the lower values obtained near to saturation conditions, $R_{L,t}(i)$, was observed for both thorium and cerium releases and all the firing temperatures considered. It was already described for $Th_{1-x}U_xO_2$ and $Ce_{1-x}Nd_xO_{2-x/2}$ solid-solutions and assigned to the existence of some perturbations associated to the establishment of saturation processes in the back-end of the initial reaction of dissolution (and to the possible formation of amorphous or crystallized neoformed phases). Conversely to that was noted for the initial normalized dissolution rates, the temperature of calcination had a smaller effect on these long-term normalized dissolution rates despite the elimination of crystal defects then the increase of crystallite size. This result could be explained by the presence of a neoformed amorphous gelatinous layer onto the surface of the leached samples. The complete characterization of such a phase that acted as a diffusion barrier during the elementary releases is under progress especially by making complementary leaching tests on dense $Th_{1-x}Ce_xO_2$ pellets.

5. CONCLUSION

$Th_{1-x}Ce_xO_2$ solid solutions samples were prepared by thermal conversion of oxalate precursors then leached by varying independently several parameters. Among them, conventional parameters (such as chemical composition, leachate acidity, leaching temperature) as well as microstructural parameters (firing temperature, crystallization state) were considered. The relative effects of these parameters on the normalized dissolution rate were examined. Conversely to that observed for $Th_{1-x}U_xO_2$ and $Ce_{1-x}Nd_xO_{2-x/2}$ solid solutions, the chemical composition did not induce strong modifications of the chemical durability of the leached samples. Either the partial order related to the proton activity ($n = 0.50 \pm 0.01$) or the activation energy ($E_A = 57 \pm 6$ kJ.mol^{-1}) determined in this work suggested that the dissolution was mainly driven by surface reactions occurring at the solid/liquid interface.

The dissolution was found to be congruent for heating temperatures below 1000 °C. Conversely, a preferential release of cerium was observed above 1100 °C probably induced by the partial reduction of Ce(IV) to Ce(III) during the heating treatment or at the solid/liquid interface during the leaching tests. Additionally, the effects of crystal defects or crystallite size were also examined. While the initial normalized dissolution rate

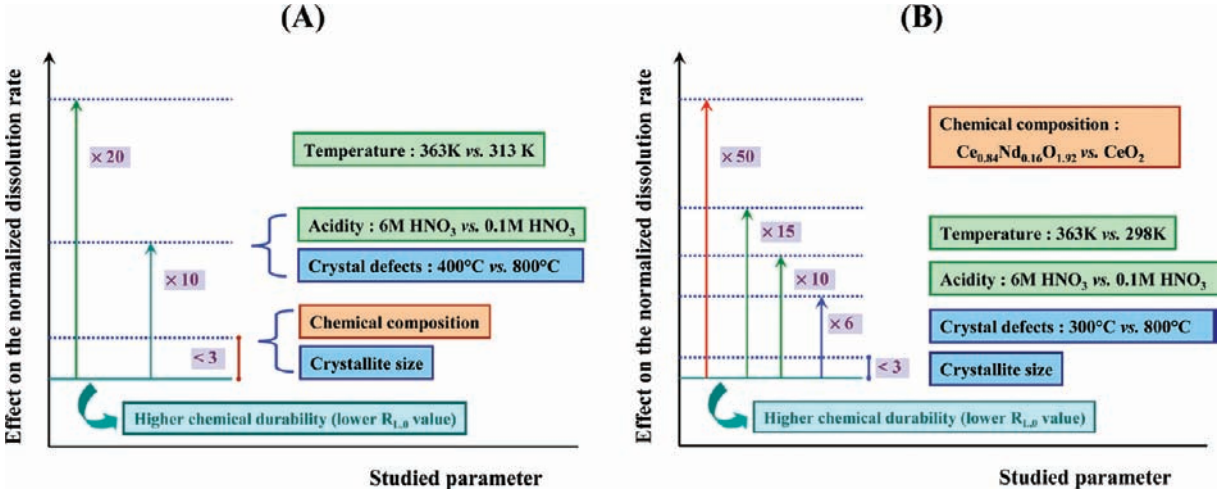

Figure 12. Influence of studied physicochemical parameters on the $Th_{1-x}Ce_xO_2$ normalized dissolution rate (A) and comparison with $Ce_{1-x}Nd_xO_{2-x/2}$[30] (B).

dx.doi.org/10.1021/ic201699t |*Inorg. Chem.* 2011, 50, 11702–11714

slightly depended on the elimination of crystal defects for firing temperatures below 800 °C, it was mainly independent of the crystallite size ($T \geq 900$ °C). Finally, near the establishment of saturation processes, the resulting normalized dissolution rates were less affected probably due to the formation of a gelatinous protective layer at the solid/liquid interface. The relative contribution of all the examined parameters is presented in Figure 12.

It is worth noting that, contrarily to that observed for $Ce_{1-x}Nd_xO_{2-x/2}$ or $Th_{1-x}U_xO_2$ solid solutions, the chemical composition did not play any significant role on the elemental releases during leaching tests. Its contribution was found to be almost similar to that of the crystallite size. Among the possible explanations of such particular behavior, one can remark that the cerium(IV) to thorium substitution occurs without any formation of oxygen vacancies such as reported for other lanthanide elements (e.g., $Ce_{1-x}Nd_xO_{2-x/2}$) and does not induce strong sensitivity to redox phenomena as for uranium(IV). On this basis, the role of microstructural parameters (such as crystal defects) appeared important to consider since they contributed to modifications in the normalized dissolution rates of the same order of magnitude than that of the leachate acidity.

Several additional physicochemical properties (such as the final density, grains size, occurrence of grains boundaries,) are now under study by leaching $Th_{1-x}Ce_xO_2$ sintered samples in order to evidence the role of additional parameters acting as microstructure modifications on the chemical durability during leaching tests. Comparative leaching tests of $Th_{1-x}Ce_xO_2$ and $Th_{1-x}U_xO_2$ are also under progress to confirm the particular effect of opposite redox reactions (reduction for Ce(IV) and oxidation for U(IV)) during the dissolution processes.

■ ASSOCIATED CONTENT

Supporting Information. Results of TGA/DTA experiments, Rietveld plot of $Th_{0.81}Ce_{0.19}O_2$, variation of unit cell parameter for $Th_{1-x}Ce_xO_2$ solid solutions, variation of the crystallite size versus the reciprocal heating temperature and normalized dissolution rates obtained during the dissolution of $Th_{1-x}Ce_xO_2$ solid solutions for several compositions. This material is available free of charge via the Internet at http://pubs.acs.org.

■ AUTHOR INFORMATION

Corresponding Author

*Phone: + 33 4 66 33 92 05. Fax: + 33 4 66 79 76 11. E-mail: nicolas.dacheux@univ-montp2.fr.

■ ACKNOWLEDGMENT

The authors would like to thank Johann Ravaux and Renaud Podor (ICSM/LM2E) for making the in situ HT-ESEM experiments and the reviewers for their constructive comments. They also thank the MATINEX French Research Group (*Innovative materials in extreme conditions*, CEA/CNRS/AREVA/EDF/French Universities) included in the PACEN Program for their subsequent financial support. This work also benefited from financial support of the French National Research Agency (ANR, project # ANR-08-BLAN-0216) and from the CNRS Interdisciplinary Research Program MaProSu (Matériaux et Procédés de Remplacement/Substitution).

■ REFERENCES

(1) Ichimiya, M.; Sagayama, Y. T. *Am. Nucl. Soc.* **2004**, *90*, 46–47.
(2) Hoffelner, W. *Chimia* **2005**, *59*, 977–982.
(3) Tommasi, J.; Delpech, M.; Groullier, J. P.; Zaetta, A. *Nucl. Technol.* **1995**, *111*, 133–148.
(4) Xiao, H. Y.; Weber, W. J. *J. Phys. Chem. B* **2011**, *115*, 6524–6533.
(5) Akie, H.; Muromura, T.; Takano, H.; Matsuura, S. *Nucl. Technol.* **1994**, *107*, 182–191.
(6) Sevik, C.; Çağin, T. *Phys. Rev. B* **2009**, *80*, 014108.
(7) Shein, I. R.; Shein, K. I.; Ivanovskii, A. L. *J. Nucl. Mater.* **2007**, *361*, 69–77.
(8) Buisson, P. PhD thesis GRE1-0519, University Grenoble 1, 1999.
(9) Arab-Chapelet, B.; Grandjean, S.; Nowogrocki, G.; Abraham, F. *J. Alloy. Compd.* **2007**, *444*−*445*, 387–390.
(10) Matthews, R. B.; Davies, N. C. OSTI Technical Report, no. PNL3210, Office of Scientific and Technical Information, U.S. Dept. Of Energy, Oak Ridge, TN, 1979.
(11) Altaş, Y.; Tel, H. *J. Nucl. Mater.* **2001**, *298*, 316–320.
(12) Yildiz, Ö. *J. Nucl. Mater.* **2007**, *366*, 266–271.
(13) Hubert, S.; Barthelet, K.; Fourest, B.; Lagarde, G.; Dacheux, N.; Baglan, N. *J. Nucl. Mater.* **2001**, *297*, 206–213.
(14) Mitra, N. K.; Mahapatra, S. S.; Chattopadhyay, A. K. *J. Ind. Chem. Soc.* **1983**, *60*, 499–501.
(15) Hingant, N.; Clavier, N.; Dacheux, N.; Barre, N.; Hubert, S.; Obbade, S.; Taborda, F.; Abraham, F. *J. Nucl. Mater.* **2009**, *385*, 400–406.
(16) Hingant, N.; Clavier, N.; Dacheux, N.; Hubert, S.; Barré, N.; Podor, R.; Aranda, L. *Powder Technol.* **2011**, *208*, 454–460.
(17) Vandenborre, J.; Grambow, B.; Abdelouas, A. *Inorg. Chem.* **2010**, *49*, 8736–8748.
(18) Heisbourg, G.; Hubert, S.; Dacheux, N.; Ritt, J. *J. Nucl. Mater.* **2003**, *321*, 141–151.
(19) Heisbourg, G.; Hubert, S.; Dacheux, N.; Purans, J. *J. Nucl. Mater.* **2004**, *335*, 5–13.
(20) Hubert, S.; Heisbourg, G.; Dacheux, N.; Moisy, P. *Inorg. Chem.* **2008**, *47*, 2064–2073.
(21) Greiling, H. D.; Lieser, K. H. *Radiochim. Acta.* **1984**, *35*, 79–89.
(22) Fournier, S. In Etude de la dissolution des oxydes mixtes $(U,Pu)O_2$ à forte teneur en plutonium, PhD, no. 00 MON2 0203, Université Montpellier II, 2000.
(23) Nikitina, G. P.; Zhukova, I. N.; Egorova, V. P. *Radiochemistry* **1995**, *37*, 193–196.
(24) Uriarte, A. L.; Rainey, R. H. In Dissolution of high-density UO_2, PuO_2 and UO_2-PuO_2 pellets in inorganic acids, Technical Report ORNL-3695, DOI:10.2172/4652087, 1965.
(25) Juillet, F.; Adnet, J. M.; Gasgnier, M. J. *Radioanal. Nucl. Chem.* **1997**, *224*, 137–143.
(26) Berger, P. In Etude du mécanisme de dissolution par oxydoréduction chimique et électrochimique des bioxydes d'actinides (UO_2, NpO_2, PuO_2, AmO_2) en milieu aqueux acide, PhD, no. 1988 PA06 6073, Université Paris VI, 1988.
(27) Machuron-Mandard, X.; Madic, C. *J. All. Compd.* **1994**, *213*-*214*, 100–105.
(28) Joret, L.; Cote, G.; Bauer, D. *Hydrometallurgy* **1997**, *45*, 1–12.
(29) Nikitina, G. P.; Gridasov, G. C.; Listopadov, A. A.; Zhukova, I. N.; Yakovlev, V. V. *Radiochemistry* **1995**, *37*, 365–371.
(30) Claparède, L.; Clavier, N.; Dacheux, N.; Moisy, P.; Podor, R.; Ravaux, J. *Inorg. Chem.* **2011**, *50*, 9059–9072.
(31) Thomas, A. C.; Dacheux, N.; Le Coustumer, P.; Brandel, V.; Genet, M. *J. Nucl. Mater.* **2000**, *281*, 91–105.
(32) Lasaga, A. C. *J. Geophys. Res.* **1989**, *89*, 4009–4025.
(33) Clavier, N.; du Fou de Kerdaniel, E.; Dacheux, N.; Le Coustumer, P.; Drot, R.; Ravaux, J.; Simoni, E. *J. Nucl. Mater.* **2006**, *349*, 304–316.
(34) Dacheux, N.; Clavier, N.; Ritt, J. *J. Nucl. Mater.* **2006**, *349*, 291–303.
(35) Dacheux, N.; du Fou de Kerdaniel, E.; Clavier, N.; Podor, R.; Aupiais, J.; Szenknect, S. *J. Nucl. Mater.* **2010**, *404*, 33–43.
(36) Walther, J. V. *Am. J. Sci.* **1996**, *296*, 693–728.
(37) Ganor, J.; Mogollon, J. L.; Lasaga, A. C. *Geochim. Cosmochim. Acta* **1995**, *59*, 1037–1052.

(38) Pokrovsky, O. S.; Schott, J. *Geochim. Cosmochim. Acta* **2000**, *64*, 3313–3325.
(39) Furrer, G.; Stumm, W. *Geochim. Cosmochim. Acta* **1991**, *55*, 2193–2201.
(40) Chou, L.; Wollast, R. *the Chemistry of Weathering*, Drever J. I., Ed.; Kluwer Academic Publishers: Dordrecht, 1985.
(41) Chou, L.; Wollast, R. *Am. J. Sci.* **1985**, *258*, 963–993.
(42) Furrer, G.; Stumm, W. *Geochim. Cosmochim. Acta* **1986**, *50*, 1847–1860.
(43) Blum, A. E.; Lasaga, A. C. *Nature* **1988**, *331*, 431–433.
(44) Robisson, A. C.; Dacheux, N.; Aupiais, J. *J. Nucl. Mater.* **2002**, *306*, 134–146.
(45) Eyring, H. *J. Chem. Phys.* **1935**, *3*, 107–115.
(46) Aagaard, P.; Helgeson, H. C. *Am. J. Sci.* **1982**, *282*, 237–285.
(47) Grenthe, I.; Puigdomenech, I. *Modelling in Aquatic Chemistry*; OECD Publications: Paris, 1997.
(48) Bruno, J.; Casas, I.; Puigdomènech, I. *Geochim. Cosmochim. Acta* **1990**, *55*, 647–658.
(49) De Pablo, J.; Casas, I.; Gimenez, J.; Molera, M.; Rovira, M.; Duro, L.; Bruno, J. *Geochim. Cosmochim. Acta* **1999**, *63*, 3097–3103.
(50) Brandel, V.; Dacheux, N.; Genet, M.; Podor, R. *J. Solid State Chem.* **2001**, *159*, 139–148.
(51) Clavier, N.; Hingant, N.; Rivenet, M; Obbade, S.; Dacheux, N.; Barre, N.; Abraham, F. *Inorg. Chem.* **2010**, *49*, 1921–1931.
(52) Joseph, C.; Varghese, G.; Ittyachen, A. *J. Therm. Anal. Calorim.* **1998**, *52*, 517–522.
(53) Ollendorff, N.; Weigel, F. *Inorg. Nucl. Chem. Lett.* **1969**, *5*, 263–269.
(54) Arab-Chapelet, B.; Grandjean, S.; Nowogrocki, G.; Abraham, F. *J. Alloys Compd.* **2007**, *444*−*445*, 387–390.
(55) Arab-Chapelet, B.; Grandjean, S.; Nowogrocki, G.; Abraham, F. *J. Nucl. Mater.* **2008**, *373*, 259–268.
(56) Raje, N.; Riddy, A. V. R. *Thermochim. Acta* **2010**, *505*, 53–58.
(57) Ubaldini, A.; Artini, C.; Costa, G. A.; Carnasciali, M. M.; Masini, R. *J. Therm. Anal. Calorim.* **2006**, *84*, 207–211.
(58) Higashi, K.; Sonoda, K.; Ono, H.; Sameshima, S.; Hirata, Y. *J. Mater. Res.* **1999**, *14*, 957–967.
(59) Finger, L. W. *J. Appl. Crystallogr.* **1998**, *31*, 111.
(60) Roisnel, T.; Rodriguez-Carvajal, J. *Mater. Sci. Forum* **2001**, *378*−*381*, 118–123.
(61) Barret, E. P.; Joyner, L. G.; Halenda, P. H. *J. Am. Chem. Soc.* **1951**, *73*, 373–380.
(62) Dacheux, N.; Le Du, J. F.; Brandel, V.; Genet, M.; Decambox, P.; Moulin, C. *New J. Chem.* **1996**, *20*, 507–514.
(63) Balboul, B. A. A.; Myhoub, A. Y. Z. *J. Anal. Appl. Pyrol.* **2010**, *89*, 95–101.
(64) Dash, S.; Krishnan, R.; Kamruddin, M.; Tyagi, A. K.; Raj, B. *J. Nucl. Mater.* **2001**, *295*, 281–289.
(65) Horlait, D.; Claparède, L.; Clavier, N.; Szenknect, S.; Dacheux, N.; Ravaux, J.; Podor, R. *Inorg. Chem.* **2011**, *50*, 7150–7161.
(66) Shannon, R. D. *Acta Cryst. A.* **1976**, *32*, 751–767.
(67) Ostwald, W. Z. *Phys. Chem.* **1897**, *22*, 289–302.
(68) Le Coustumer, P.; Monthioux, M.; Oberlin, A. *J. Eur. Ceram. Soc.* **1993**, *11*, 95–103.
(69) Jarcho, M.; Bolen, C. H.; Thomas, M. B.; Bobick, J.; Kay, J. F.; Doremus, R. H. *J. Mater. Sci.* **1976**, *11*, 2027–2035.
(70) Chen, J. C.; Chen, W. C.; Tien, Y. C.; Shih, C. J. *J. Alloys Compd.* **2010**, *496*, 364–369.
(71) Dollimore, D. *Thermochim. Acta* **1987**, *117*, 331–363.
(72) Osaka, M.; Miwa, S.; Kurosaki, K.; Uno, M.; Yamanaka, S. *J. Nucl. Mater.* **2011**, *408*, 285–288.
(73) Aurousseau, M.; Lapicque, F.; Storck, A. *Ind. Eng. Chem. Res.* **1994**, *33*, 191–196.
(74) Ruas, A.; Pochon, P.; Simonin, J. P.; Moisy, P. *Dalton Trans.* **2010**, *39*, 10148–10153.
(75) Krawetz, A. Raman spectral study of equilibria in aqueous solutions of nitric acid, PhD Thesis, University of Chicago, 1955.
(76) Terry, B. *Hydrometallurgy* **1983**, *11*, 315–344.